Simulation of a tunable optically pumped terahertz intersubband laser with diluted magnetic semiconductors

Miloš Popadić
Faculty of Electrical Engineering, University of Belgrade, Bulevar Kralja Aleksandra 73, 11120 Belgrade, Serbia and Montenegro and Laboratory of ETCM, Department of Microelectronics, DIMES, Delft Univesity of Technology, Feldmannweg 17, 2628CT Delft, The Netherlands

Vitomir Milanović[a)]
Faculty of Electrical Engineering, University of Belgrade, Bulevar Kralja Aleksandra 73, 11120 Belgrade, Serbia and Montenegro

Zoran Ikonić and Dragan Indjin
School of Electronic and Electrical Engineering, University of Leeds, Leeds LS2 9JT, United Kingdom

(Received 17 February 2006; accepted 11 July 2006; published online 10 October 2006)

A simulation of an optically pumped laser based on a $ZnSe/Zn_{1-y}Cd_ySe$ double quantum well with a $Zn_{1-x}Mn_xSe$ diluted magnetic semiconductor barrier is presented. Giant Zeeman splitting in diluted magnetic semiconductors leads to splitting of electronic states, which in turn leads to tunability of laser wavelength by external magnetic field. Tunability is predicted throughout the wavelength range between 60 and 72 μm at low temperatures. © *2006 American Institute of Physics*. [DOI: 10.1063/1.2355544]

I. INTRODUCTION

Diluted magnetic semiconductors (DMSs) are semiconductor alloys partly composed of magnetic materials. Due to their unique, qualitatively different behavior from that of non-DMSs, they attract an increasing scientific interest.[1–6] Several interband devices utilizing DMS were proposed,[7–10] but very few attempts were made in designing quantum intersubband devices based on DMS.[11] Application of external magnetic field leads to field-dependent splitting of the DMS conduction band edge. Variation of the magnetic field, material composition, or temperature changes the material parameters, which can be transformed into tunability of output characteristics via appropriate device design.[12,13] Tunable lasers in the terahertz range would be very useful spectroscopic tools, with numerous molecular lines in this range, and would find application in fields such as medicine, astronomy, environmental protection, security technology, etc. A lot of research is devoted to the development of terahertz quantum cascade lasers[14–17] and quantum well infrared photodetectors.[18–20] The lasers are essentially fixed-wavelength devices, possibly tunable only within a fraction of the spontaneous emission linewidth.

In this paper we present an approach to designing tunable intersubband lasers, based on double quantum wells with a $Zn_{1-x}Mn_xSe$ DMS barrier, which we chose due to its rather thoroughly investigated properties. The mechanism of tunability is that the wave functions of different subbands have generally different overlaps with the DMS portion of the structure, and will thus experience different changes of the potential when the external magnetic field varies, which results in field-dependent transition energies. We consider an optically pumped laser, which is simpler than an injection pumped laser, with the advantages of selectivity in populating higher energy levels and absence of carrier losses at contacts. We set up a model of electron dynamics, which includes phonon scattering transitions and optical transitions, and use it to predict the device feasibility.

II. THEORETICAL CONSIDERATIONS

A. Conduction band edge and giant Zeeman splitting

The structures considered here comprise two non-DMS $Zn_{1-y}Cd_ySe$ quantum wells separated by a thin DMS $Zn_{1-x}Mn_xSe$ barrier and embedded in ZnSe bulk. The height of the barrier is above the ZnSe bulk and was modeled as a graded interface between the barrier and the wells. The graded interface represents the diffusion region, taken to be 2 ML (monolayers) thick. Band offsets of $Zn_{1-x}Mn_xSe$ and $Zn_{1-y}Cd_ySe$ relative to ZnSe are, to a good approximation, linear functions of Mn and Cd concentrations[11]

$$\Delta E_{cx} = 520.7x \text{ meV},$$

$$\Delta E_{cy} = -780y \text{ meV}. \quad (1)$$

The graded interface intermixing region is regarded as a $Zn_{(1-x)(1-y)}Cd_yMn_{x(1-y)}Se$ alloy with a band offset

$$\Delta E_{cxy} = [520.7x(1-y) - 780y] \text{ meV}. \quad (2)$$

The $3d$ orbital of Mn, the typical constituent of DMS such as $Zn_{1-x}Mn_xSe$, is only half filled, with all five electrons having the same spin orientation. The external magnetic field partly orders electron spins in different Mn ions, and the spin-spin interaction between bound Mn electrons and free subband electrons in DMS then introduces a spin dependent potential acting on free electrons, stronger than that caused

[a)]Electronic mail: milanovic@etf.bg.ac.yu

by the magnetic field acting on spins themselves. This is known as the giant Zeeman splitting of the conduction band edge.[2] The amount of splitting is[2,9–11,21]

$$\Delta E_c = \pm \alpha N_0 \bar{x} \langle S_z \rangle, \tag{3}$$

where the "+" and "−" signs apply to opposite spins, α is the *sp-d* exchange integral for the conduction band, N_0 is the cation density, $\bar{x}$ is the effective Mn^{2+} concentration, and $\langle S_z \rangle$ is the thermal average of Mn^{2+} spin, given by the modified Brillouin function[11]

$$\langle S_z \rangle = \frac{5}{2} B_{5/2}\left[\frac{5/2 g^* \mu_B B}{k(T+T_0)} \right],$$

where $g^* \approx 2$ is the Landé factor, μ_B is the Bohr magneton, and T_0 is the phenomenological fitting parameter known as effective temperature.

The effective Mn concentration is introduced due to paramagnetic interaction between neighboring ions, and in the limit of $x=1$ it tends to $\bar{x}=0$. The $\bar{x}(x)$ dependence has a maximum approximately at $x=0.2$, reaching $\bar{x}=0.04$.[9] However, in the intermixed barrier-well interface region the number of nearest neighbors is reduced, enhancing the giant Zeeman splitting, with effective Mn concentration taking the value $\bar{x}=0.12$ for $x=0.2$. This enhancement makes a substantial contribution to the giant Zeeman splitting at DMS/non-DMS interfaces, requiring the intermixed region at interfaces to be accounted for.

B. Electronic states

The subband energies E and envelope wave functions $\eta(z)$ were found within the effective mass approximation, with the potential given by (1) and (2), and assuming a constant effective mass m across the structure, which is a reasonable approximation for the materials with Mn and Cd concentrations involved. The electrostatic potential of free electrons and donor ions was neglected. At zero magnetic field the in-plane dispersion of subbands is parabolic, starting with the subband bottom energies E_{i0}. However, in a magnetic field perpendicular to the quantum well layers (i.e., parallel to the z axis), the in-plane wave vector continuum of states in each subband splits into discrete, infinitely degenerate, set of Landau levels[22] (LLs) with energies

$$E_{i,j} = \left(j + \frac{1}{2} \right) \hbar \omega_c + E_{i0} \tag{4}$$

and the corresponding wave functions

$$\psi = e^{ik_x x} e^{-(eB)/(2\hbar)[y+(\hbar k_x)/(eB)]^2} H_n\left[\sqrt{\frac{eB}{\hbar}}\left(y + \frac{\hbar k_x}{eB} \right) \right] \eta(z), \tag{5}$$

where $\omega_c = eB/m$, and H_n are Hermite polynomials. The sets of LLs originating from the same subband will be denoted as the corresponding subsets.

C. Electron-phonon scattering

In nonzero magnetic field the electron-phonon scattering rates take a different form from the zero-field case. The scattering rate with confined phonon modes has been derived as[23]

$$W = \frac{\omega_0 e^2}{d}\left(\frac{1}{\varepsilon_\infty} - \frac{1}{\varepsilon_0} \right) \sum_n P_n^2 \delta[\hbar\omega_c(\nu_i - \nu_f) + E_{i0} - E_{f0} - \hbar\omega_0] \times \int_0^\infty q_\parallel \frac{|F(q_\parallel, \nu_i, \nu_f)|^2 dq_\parallel}{\alpha_n^2 + q_\parallel^2}, \tag{6}$$

where ω_0 is the phonon frequency, d is the confining layer thickness, P_n is the overlap integral along z axis $P_n = \int_0^d \eta_f^*(z) \sin(\alpha_n z) \eta_i(z) dz$, $\alpha_n = n\pi/d$, ν is the LL index, and F is the overlap integral in the x-y plane

$$|F(q_\parallel, \nu_i, \nu_f)|^2 = e^{-q_\parallel^2/2\beta^2} \frac{\nu_i!}{\nu_f!}\left(\frac{q_\parallel^2}{2\beta^2} \right)^{\nu_f - \nu_i} \left[L_{\nu_i}^{\nu_f - \nu_i}\left(\frac{q_\parallel^2}{2\beta^2} \right) \right]^2,$$

where $\beta = eB/\hbar$, and L_n^k is the associated Laguerre polynomial.

Considering the bulk phonons as confined phonon modes in the limit $d \to \infty$, the summation in (6) changes to integration, yielding

$$W_{if}^{\mathrm{LO}\pm} = \frac{\omega_0 e^2}{\pi}\left(\frac{1}{\varepsilon_\infty} - \frac{1}{\varepsilon_0} \right) \delta[\hbar\omega_c(\nu_i - \nu_f) + E_{zi} - E_{zf} - \hbar\omega_0] \times \left[N_0(\hbar\omega_0) + \frac{1}{2} \pm \frac{1}{2} \right] \times \int_0^\infty \int_0^\infty P^2(q_z) q_\parallel \frac{|F(q_\parallel, \nu_i, \nu_f)|^2}{q_z^2 + q_\parallel^2} dq_\parallel dq_z, \tag{7}$$

with α_n substituted in notation by q_z and with the factor $N_0(\hbar\omega_0) + 1/2 \pm 1/2$ added, where N_0 is the phonon number, according to the Bose-Einstein distribution. In actual calculation the Gaussian distribution function was used instead of the delta function[24]

$$\delta(x) = \frac{1}{2\sqrt{\pi}\sigma} e^{-x^2/4\sigma^2}, \tag{8}$$

where

$$\sigma = \begin{cases} \sigma_A = \sigma_0 \sqrt{B/2} & \text{for intrasubset transitions } (\nu_i \neq \nu_f, E_{i0} = E_{f0}) \\ \sigma_B = \sqrt{\pi}\Gamma/2 & \text{for Landau level conserving transitions } (\nu_i = \nu_f, E_{i0} \neq E_{f0}) \\ \sigma_C = \sqrt{\sigma_A^2 + \sigma_B^2} = \sqrt{\sigma_0^2 B/2 + \pi\Gamma^2/4} & \text{in other cases,} \end{cases}$$

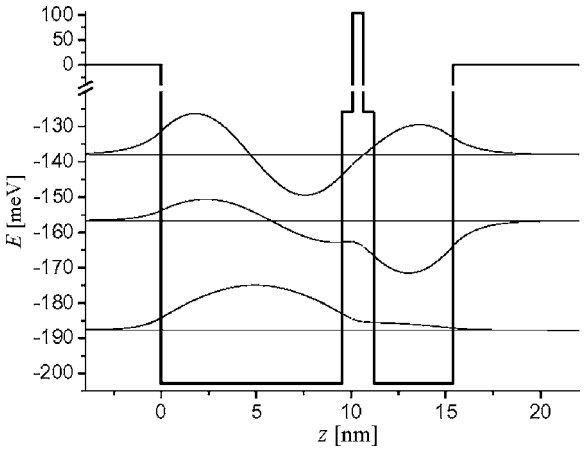

FIG. 1. Conduction band potential profile along the z axis and the envelope wave functions of the first three subbands, shown at the corresponding energy level positions. The energy difference between the first two subbands is equal to LO phonon energy. Energy difference between the second and third subband is approximately 20 meV, which corresponds to the lasing frequency of 5 THz.

where $\sigma_0=1$ meV, and Γ was taken as 15% of the transition energy.

For the case of acoustic phonons, we derived the transition rates in the form[25]

$$W_{if}^{A\pm}=\frac{D_A^2(E_i-E_f)^2}{\pi\hbar^3\rho v_s^4}\left[N_0(E_i-E_f)+\frac{1}{2}\pm\frac{1}{2}\right]\times\int_0^{q_{z\,\max}}|P(q_z)|^2|F(q_{\|0})|^2dq_z, \tag{9}$$

where D_A is the acoustic deformation potential, ρ is the density, v_s is the sound velocity, $q_{z\,\max}=|(E_i-E_f)/\hbar v_s|$, $q_{\|0}=\sqrt{[(E_i-E_f)/\hbar v_s]^2-q_z^2}$, and other symbols are as in (7).

D. Rate equations

In the conventional intersubband lasers (without the magnetic field) the electron distribution is found by solving the set of rate equations, which use the scattering rates between all pairs of subbands. Such scattering rates are in fact weight averaged over the in-plane wave vector, assuming the distribution within a subband is Fermi-Dirac-like, and the number of rate equations is then equal to the number of relevant subbands. In a magnetic field, with all the states being discrete (LLs), there is no averaging to be performed, but the number of states to account for is much larger. Electron densities in LLs generally decrease with their index (i.e., energy), though not necessarily in a Fermi-Dirac-like manner as they do in continuous subbands, and only a limited number of LLs really have to be accounted for. The number of LLs to be taken can thus be roughly estimated from their spacing, which depends on the field. Since this spacing increases linearly with the field, it is very difficult to get the zero-field limit in a formal manner because the number of states becomes too large for numerical calculation.

In the system of rate equations, the electron-phonon scattering rates were calculated for each pair of LLs, while the optical transitions are allowed only among the LLs of the same index (assuming z-polarized light). Spin-flip transitions are less significant than phonon scattering[26] and were neglected, implying that electron distribution between spin-up and spin-down states corresponds to equilibrium. This was calculated assuming Fermi distribution among LLs, with a common Fermi level[11]

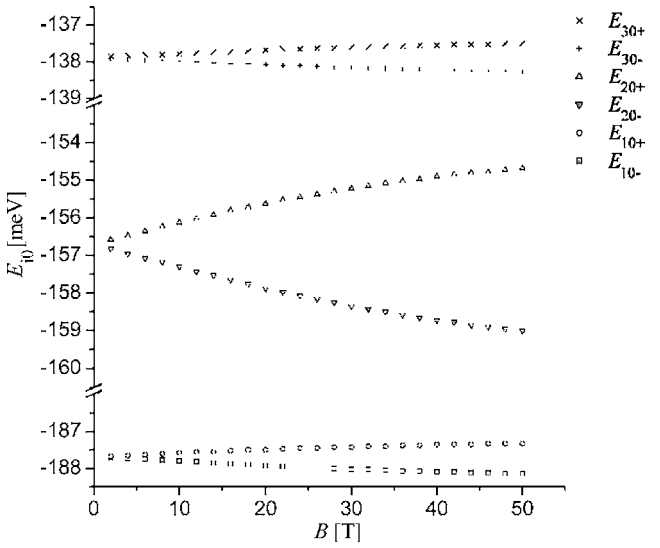

FIG. 2. Positions of subband bottoms (E_{i0}) as a function of magnetic field for the chosen structure at $T=77$ K. Zero of the energy axis is at the bottom of the conduction band edge in ZnSe; the "+" and "−" superscripts correspond to opposite spins.

$$n_{i,j}(E_{i,j})=\frac{eB}{2\pi\hbar}\frac{1}{e^{(E_{i,j}-E_F)/kT}+1}, \tag{10}$$

and with the total electron density

$$N_S=\sum_{i,j}n_{i,j}. \tag{11}$$

Similar to the case of zero magnetic field, the electron densities in LLs are determined by electron transition rates, used in two independent sets of nonlinear rate equations for electrons with the two spin orientations[27,28]

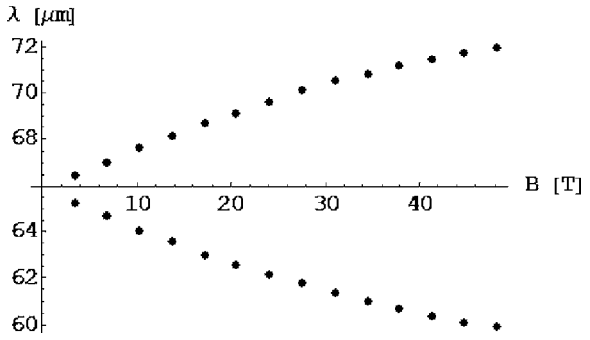

FIG. 3. The lasing transition wavelength as a function of magnetic field for the chosen structure at $T=77$ K.

$$\frac{dn_f}{dt} = 0 = \sum_{i,f,i\neq f} n_i W_{i,f} - n_f \sum_{i,f,i\neq f} W_{f,i} + \sigma_{13f}\Phi(n_f - n_c), \tag{12}$$

where the subscripts i and f run over all LL subsets with one spin orientation, and the transition rates are multiplied by the probability of finding an empty final state, i.e., accounting for Pauli exclusion principle

$$W_{i,f} = (W_{if}^{\mathrm{LO}\pm} + W_{if}^{A\pm})[1 - f_{\mathrm{FD}}(E_f, E_{Ff})], \tag{13}$$

and

$$\sigma_{13f} = \begin{cases} \sigma_{13} & \text{with } f \text{ representing a level from the third subset} \\ 0 & \text{with } f \text{ representing a level from the second subset} \\ -\sigma_{13} & \text{with } f \text{ representing a level from the first subset,} \end{cases} \tag{14}$$

with n_c denoting the electron density in the "complementary" LL, i.e., the one with the same index from the first (third) subset in the case of f representing a level from the third (first) subset, respectively.

From the calculated electron densities, the gain amounts to[29]

$$g = \sigma_{23}\frac{n_3 - n_2}{L_W}, \tag{15}$$

where L_W is the total width of the structure.

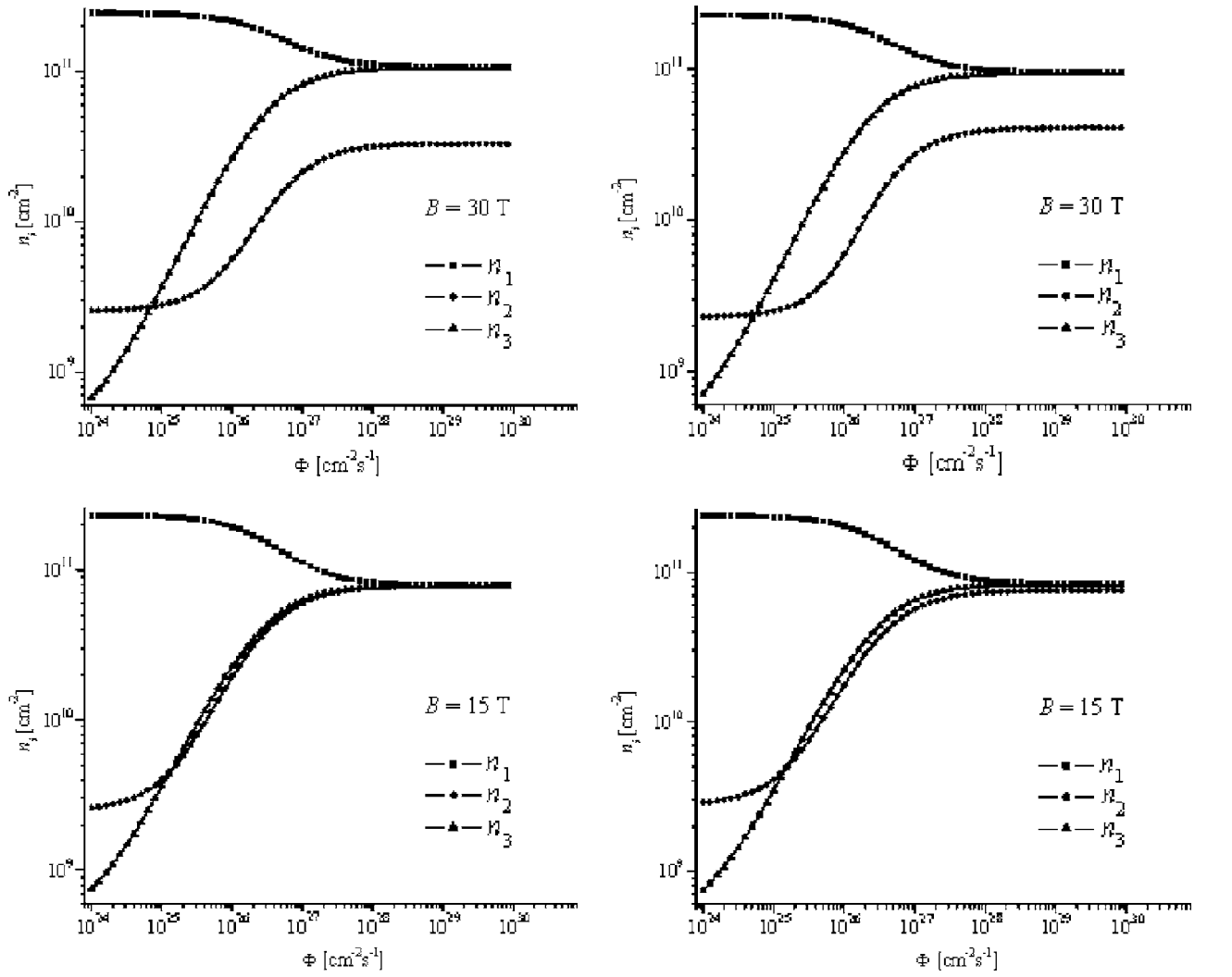

FIG. 4. The electron densities in LL subsets of the designed structure vs the pump flux dependence at $T=77$ K, for spin-up (left) and spin-down electrons (right), calculated for $B=30$ T (top row) and $B=15$ T (bottom row).

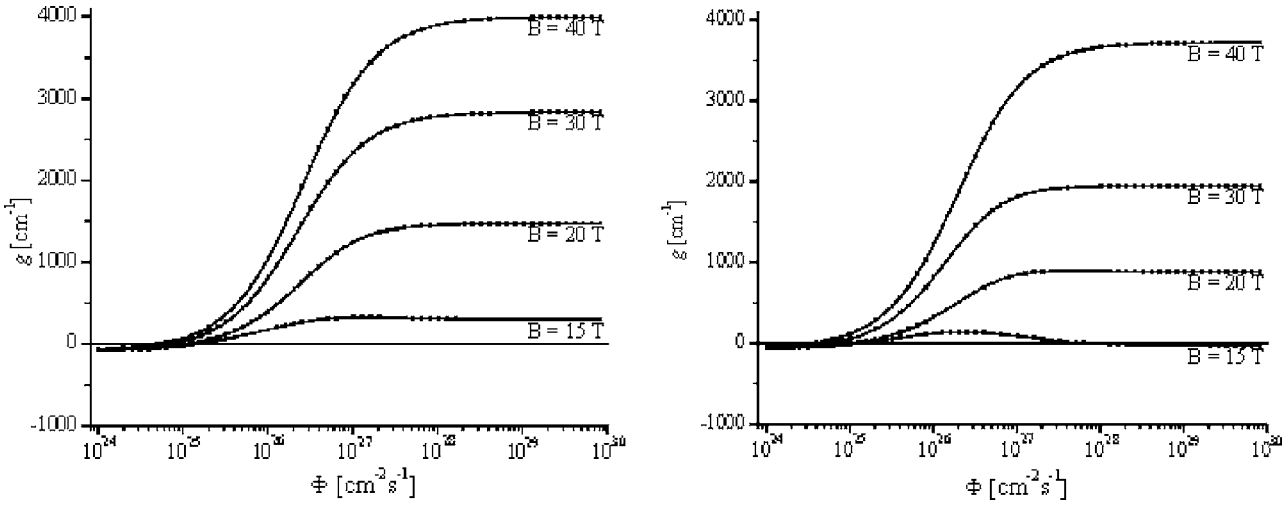

FIG. 5. The gain vs pump flux dependence at $T=77$ K for different values of the magnetic field, calculated for spin-up (left) and spin-down (right) electron transitions.

III. NUMERICAL RESULTS AND DISCUSSION

In order to design a magnetic field tunable laser structure, we have varied the parameters to get a large sensitivity of the spacing between the third and second subsets, i.e., $E_{30}-E_{20}$ (the adjustable-wavelength lasing transition), and a small sensitivity of the spacing between the second and first subsets, i.e., $E_{20}-E_{10}$ (the LO phonon relaxation transition, fixed energy preferred). By varying the widths of the barrier and the quantum wells, as well as the Mn^{2+} and Cd^{2+} concentrations, the structure was optimized to give a maximal gain and a strong dependence of electronic state energies on the magnetic field. Its parameters are $a=34$ ML, $c=15$ ML, and $b=2$ ML (Fig. 1), with 1 ML=0.28 nm. The Mn and Cd concentrations are $x=0.2$ and $y=0.26$, respectively. The structure is asymmetric and thus provides a finite optical cross section for pump absorption and also for the stimulated emission. In general, all structures of this type have a pronounced splitting of the second level, as a consequence of the wave function forms (Fig. 1), and the structure with maximal sensitivity of the 3-2 transition was chosen.

The positions of subband bottoms (E_{i0}), as a function of the magnetic field at $T=77$ K, are shown in Fig. 2, and the lasing transition wavelength versus field dependence for this structure is shown in Fig. 3. Larger magnetic fields are required to get the same amount of splitting at higher temperatures.

The level population and the gain versus pump flux dependences were calculated for different magnetic fields, taking the electron surface density of $N_S=5\times10^{11}$ cm^{-2} and the lattice temperature $T=77$ K. Some results are shown in Figs. 4(a), 4(b), and 5. The gain increases with the magnetic field as a consequence of increasing transition rates between LL subsets of the lowest two levels. This follows from (7), where the overlap integral F depends on β, which increases with the magnetic field. In addition, a slight difference between spin-up and spin-down electrons is observed. In the case of spin-down electrons, the increase of the magnetic field reduces the spacing between the second and first subsets of LLs below the LO phonon energy. This adversely affects the lower laser level relaxation, while the opposite holds true for spin-up electrons, as follows from (7).

The dependence of gain on the magnetic field for two spin orientations is shown in Fig. 6 for the pump flux of $\Phi=2.5\times10^{26}$ cm^{-2} s^{-1}. The typical waveguide and mirror losses of intersubband lasers are very small in comparison to the gain obtained, and lasing can be anticipated throughout the whole range of magnetic fields. The case of small fields could not be really investigated because a large number of narrowly spaced LLs would have to be included. However, even if lasing was not possible for small magnetic fields in Fig. 6, the wide large-field region of wavelength-tunable lasing still remains.

IV. CONCLUSION

The design of an optically pumped intersubband laser based on double quantum wells with a DMS barrier was

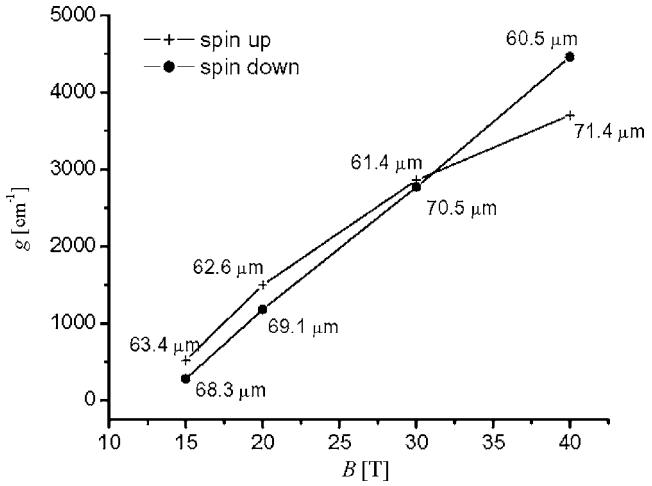

FIG. 6. The dependence of gain on the magnetic field, calculated for $\Phi=2.5\times10^{26}$ cm^{-2} s^{-1} at $T=77$ K, for both spin orientations. For every value of the magnetic field there are two lasing wavelengths which are indicated. The difference between the wavelengths increases with the magnetic field according to Fig. 3. The line connecting the actually calculated points is just the guide to the eyes.

considered, and the operation of such a device was modeled by the rate equation approach. The structure was optimized with respect to the value of gain and the frequency tunability in the range around 5 THz. High gain at high magnetic fields (at and above 15 T) was predicted at $T=77$ K, while the operation at smaller magnetic fields (below 15 T) was not investigated due to computational limitations. A considerable tunability, approximately 20% of the central frequency, could be achieved with very high magnetic fields (up to 40 T), and it is anticipated that high magnetic fields can be traded off for operation at lower temperatures, where DMSs reach saturation at even lower fields.

[1]J. A. Gaj, in *Diluted Magnetic Semiconductors*, Semiconductors and Semimetals Vol. 25, edited by J. K. Furdyna and J. Kossut (Academic, Boston, 1988).
[2]J. K. Furdyna, J. Appl. Phys. **64**, R29 (1988).
[3]H. Ohno, Science **281**, 951 (1998).
[4]H. Akinaga and H. Ohno, IEEE Trans. Nanotechnol. **1**, 19 (2002).
[5]T. Dietl, J. Magn. Magn. Mater. **272**, 1969 (2004).
[6]N. Samarath, Solid State Phys. **58**, 1 (2004).
[7]E. D. Isaacs, D. Heiman, J. J. Zayhowski, R. N. Bicknell, and J. F. Schetzina, Appl. Phys. Lett. **48**, 275 (1986).
[8]Y. Yamada, Y. Masumoto, J. T. Mullins, and T. Taguchi, Appl. Phys. Lett. **61**, 2190 (1992).
[9]S. Lee, M. Dobrowolska, J. K. Furdyna, H. Luo, and L. R. Ram-Mohan, Phys. Rev. B **54**, 16939 (1996).
[10]M. Syed, G. L. Yang, J. K. Furdyna, M. Dobrowolska, S. Lee, and L. R. Ram-Mohan, Phys. Rev. B **66**, 075213 (2002).
[11]I. Savić, V. Milanović, Z. Ikonić, D. Indjin, V. Jovanović, and P. Harrison, IEEE J. Quantum Electron. **40**, 1614 (2004).
[12]T. Wojtowicz, M. Kutrowski, G. Karczewski, and J. Kossut, Appl. Phys. Lett. **73**, 1379 (1998).
[13]I. A. Merkulov *et al.*, Phys. Rev. Lett. **83**, 1431 (1999).
[14]R. Köhler *et al.*, Nature (London) **417**, 156 (2002).
[15]M. Rochat, L. Ajili, H. Willenberg, J. Faist, H. E. Beere, A. G. Davies, E. H. Linfield, and D. A. Ritchie, Appl. Phys. Lett. **81**, 1381 (2002).
[16]B. S. Williams, H. Callebaut, S. Kumar, Q. Hu, and J. Reno, Appl. Phys. Lett. **82**, 1015 (2002).
[17]J. Alton *et al.*, Phys. Rev. B **68**, 081303(R) (2003).
[18]M. Graf, G. Scalari, D. Hofstetter, J. Faist, H. Beere, E. Linfield, D. Ritchie, and G. Davies, Appl. Phys. Lett. **84**, 475 (2004).
[19]H. C. Liu, C. Y. Song, A. J. SpringThorpe, and J. C. Cao, Appl. Phys. Lett. **84**, 4068 (2004).
[20]H. Luo, H. C. Liu, C. Y. Song, and Z. R. Wasilewski, Appl. Phys. Lett. **86**, 231103 (2005).
[21]J. A. Gaj, W. Grieshaber, C. Bodin-Deshayes, J. Cibert, G. Feuillet, Y. Merle d'Aubigne, and A. Wasiela, Phys. Rev. B **50**, 5512 (1994).
[22]L. D. Landau and E. M. Lifshitz, *Quantum Mechanics: Nonrelativistic Theory* (Pergamon, London, 1959).
[23]P. J. Turley and S. W. Teitsworth, J. Appl. Phys. **72**, 2356 (1992).
[24]J. Eisenstein, H. Stormer, V. Narayanamurti, A. Cho, A. Gossard, and C. Tu, Phys. Rev. Lett. **55**, 875 (1985).
[25]G. Sun and J. B. Khurgin, IEEE J. Quantum Electron. **29**, 1104 (1993).
[26]A. Dyson and B. K. Ridley, Phys. Rev. B **69**, 125211 (2004).
[27]V. D. Jovanovic, P. Harrison, Z. Ikonić, and D. Indjin, J. Appl. Phys. **96**, 269 (2004).
[28]Z. Ikonić, P. Harrison, and R. W. Kelsall, J. Appl. Phys. **96**, 6803 (2004).
[29]N. Vukmirović, V. D. Jovanović, D. Indjin, Z. Ikonić, P. Harrison, and V. Milanović, J. Appl. Phys. **97**, 103106 (2005).